J. Fluid Mech. (1982), *vol.* 122, *pp.* 215–234
Printed in Great Britain

Oscillatory flow inside a square cavity

By P. W. DUCK
Department of Mathematics, University of Manchester

(Received 15 October 1981)

The flow inside a square cavity, generated by a uniform oscillatory motion of the upper cavity wall, is investigated. Numerical solutions of the full unsteady Navier–Stokes equations are computed for a selection of Reynolds' numbers and frequency parameters in the range 0–600. These results show that the steady streaming component of the flow, in general, comprises two main, equal, contrarotating eddies, situated in the upper half of the cavity (one on either side of the cavity centreline) and two weaker, equal, contrarotating eddies, situated in the lower section of the cavity (again one on either side of the cavity centreline).

1. Introduction

The problem of the flow inside a rectangular cavity, generated by the steady uniform translation of one of the walls, has been of much interest in recent years, to fluid-mechanics workers and numerical analysts alike. To the former, the motion represents a simple example of steady flow involving closed streamlines, the importance of this being its relevance to separated flows. The interest to the numerical analyst is a challenging numerical problem (few analytic solutions to this type of problem are possible, even for regimes in which inertia terms are unimportant), because of the non-linearity of the (Navier–Stokes) equations of motion, and because of the presence of regions in which the solution changes rapidly.

Two of the earliest attempts at solving the (steady) square-cavity problem were made by Kawaguti (1961) and by Burggraf (1966), who presented finite-difference solutions for Reynolds numbers in the range 0–64 and 0–400 respectively. Even at these moderate Reynolds numbers, Burggraf (1966) was able to show that the results were in quantitative agreement with the prediction of Batchelor (1956) for infinite Reynolds number that the flow comprised a significant inviscid rotational core.

Since this work, a number of different numerical methods have been introduced, using the square-cavity problem as a test case (e.g. Greenspan 1968; Vahl Davis & Mallinson 1976; Shay 1981). In addition Tuann & Olson (1978) give a review of a number of other studies of this type.

One point that is made manifest repeatedly by these studies is that it is imperative to use very small mesh sizes in any differencing scheme for large Reynolds' numbers. This may be interpreted physically as meaning that there must be an acceptable number of grid points inside any boundary layers.

As noted earlier, any progress analytically on problems of this type is difficult, although Pan & Acrivos (1967) do present some analytic (and numerical) solutions for the creeping-flow solution (i.e. zero Reynolds number) for situations in which the aspect ratio of the cavity (i.e. ratio of length to height of the cavity) is either large or small.

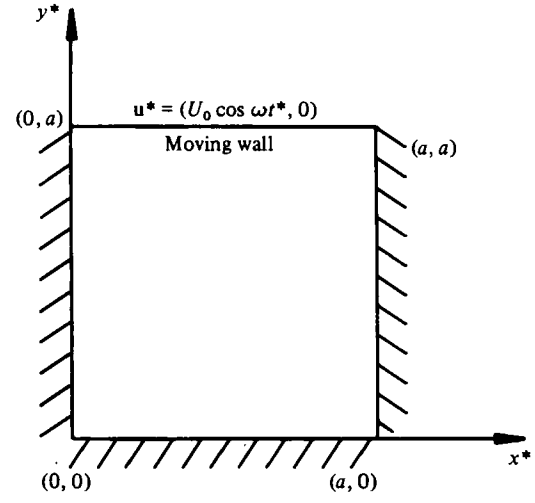

FIGURE 1. Layout.

In this paper we study the motion generated inside a square cavity, when one of the walls is performing uniform oscillatory motion, in order to gain some insight into unsteady motion involving closed streamlines. We shall pay particular attention to the 'steady streaming' arising out of the nonlinearity of the Navier–Stokes equations of motion.

Much work to date has been carried out on the steady streaming arising from purely oscillatory forced motion, although most of these studies have fallen into two categories enabling progress to be made analytically. The first of these categories is that in which the amplitude of oscillation input is very much smaller than a typical body dimension; for example, the work of Riley (1965) and Stuart (1966), who studied the flow resulting from an unbounded fluid containing a circular cylinder performing small-amplitude oscillations. (A number of other similar problems have also been attempted, in various parameter regions, and these are reviewed by Riley (1967).) The corresponding problem, but with the fluid bounded by a second, larger, fixed circular cylinder, has been investigated experimentally by Bertelsen (1974) and theoretically by Duck & Smith (1979). The second class of problem is that in which a typical surface dimension is very much smaller than the size of oscillation of the fluid particles, such as the work of Lyne (1971). In both these categories, the ratio of a typical body dimension to the typical size of fluid-particle oscillation provides a small (large) parameter, with which some form of linearization may be possible.

In the problem under consideration we concern ourselves primarily with a class of problem that requires a numerical attack (but certain asymptotic structures in various parameter limits will be noted), since no such linearization is possible.

2. Problem formulation

The layout of the problem under consideration is shown in figure 1. We assume that the flow is two-dimensional and laminar, and is described by the unsteady form of the Navier–Stokes equations, namely

$$\frac{\partial \mathbf{u}^*}{\partial t^*} + (\mathbf{u}^* . \nabla)\, \mathbf{u}^* = \nu \nabla^2 \mathbf{u}^* - \nabla p^*, \tag{2.1}$$

and by continuity,
$$\nabla . \mathbf{u}^* = 0, \tag{2.2}$$
where $\mathbf{u}^*$ is the dimensional velocity vector, p^* is the dimensional pressure, and ν is the kinematic viscosity. We now introduce the non-dimensional quantities
$$\mathbf{u} = \mathbf{u}^*/U_0, \quad x = x^*/a, \quad y = y^*/a, \quad t = \omega t^*, \tag{2.3}$$
and introduce a (non-dimensional) stream function by
$$\mathbf{u} = (\psi_y, -\psi_x). \tag{2.4}$$

Combining the Navier–Stokes equations, continuity and (2.4) yields
$$\beta \frac{\partial(\nabla^2\psi)}{\partial t} + R\frac{\partial(\nabla^2\psi, \psi)}{\partial(x, y)} = \nabla^4\psi. \tag{2.5}$$
Here R is a Reynolds number, namely $U_0 a/\nu$, and β is a frequency parameter, namely $\omega a^2/\nu$. Physically, an increase in the size of R may be interpreted as an increase in the amplitude of oscillation of the driving wall, whilst an increase in the size of β corresponds to a higher frequency of oscillation of the moving wall. The (non-dimensional) boundary conditions are then
$$\left.\begin{aligned} \psi &= 0 \quad (x = 0, 1; \quad 0 \leqslant y \leqslant 1), \\ \psi &= 0 \quad (y = 0, 1; \quad 0 \leqslant x \leqslant 1); \end{aligned}\right\} \tag{2.6}$$
$$\left.\begin{aligned} \psi_y &= 0 \quad (y = 0; \quad 0 \leqslant x \leqslant 1), \\ \psi_y &= \cos t \quad (y = 1; \quad 0 \leqslant x \leqslant 1), \\ \psi_x &= 0 \quad (x = 0, 1; \quad 0 \leqslant y \leqslant 1). \end{aligned}\right\} \tag{2.7}$$
In § 3 we consider a numerical solution to (2.5)–(2.7).

3. Method of solution

We now consider the numerical solution of the mathematical problem posed by (2.5)–(2.7). Following previous work on the corresponding steady problem, we find it convenient to introduce a new quantity
$$\zeta = -\nabla^2\psi \tag{3.1}$$
(equivalent to the vorticity). Equation (2.5) may then be split into two second-order equations, namely (3.1) and
$$\beta\frac{\partial\zeta}{\partial t} + R\frac{\partial(\zeta, \psi)}{\partial(x, y)} = \nabla^2\zeta. \tag{3.2}$$

Since the fluid motion is forced by a purely harmonic wall motion, we assume that the solution to the problem is also periodic (i.e. there are no secular solutions), and so the solution may be decomposed in time into a Fourier series:
$$\psi(x, y, t) = \sum_{n=-\infty}^{\infty} \psi_n(x, y)\, e^{\mathrm{i}nt}, \tag{3.3a}$$
$$\zeta(x, y, t) = \sum_{n=-\infty}^{\infty} \zeta_n(x, y)\, e^{\mathrm{i}nt}, \tag{3.3b}$$
where we must have
$$\psi_{-n} = \psi_n^*, \quad \zeta_{-n} = \zeta_n^* \tag{3.4}$$
(* denotes complex conjugate).

An alternative approach to treating time dependence would be to use a time-marching method, starting from some prescribed initial conditions. Indeed, an early attempt to study the steady flow inside rectangular cavities by Simuni (1964) involved just such a procedure, the steady solution being considered as the large-time limit of the unsteady equations of motion. However, our Fourier series approach is thought to have a number of advantages, including the following. (i) An automatic 'building in' of the expected periodicity of the solution, bypassing any transient solutions. (ii) The method gives a better insight into the different components of the solution; in particular the steady streaming component of the flow is evaluated during the course of the computation (marching methods would require an additional integration over a full cycle in order to evaluate the steady streaming). (iii) Certain symmetries in the solution may be exploited for the case of a purely oscillatory upper wall, which effectively halves the solution domain.

Having expanded ψ and ζ in the form (3.3), we now have the following system to solve for $n = 0, \pm 1, \pm 2, \ldots$:

$$\zeta_n + \nabla^2 \psi_n = 0, \tag{3.5a}$$

$$ni\beta\zeta_n - \nabla^2\zeta_n + R(\psi_{n,y}\zeta_{0,x} - \zeta_{n,y}\psi_{0,x}) = R \sum_{\substack{j=-\infty \\ j \neq n}}^{\infty} [\psi_{n-j,x}\zeta_{j,y} - \psi_{j,y}\zeta_{n-j,x}], \tag{3.5b}$$

subject to

$$\left.\begin{aligned} \psi_n &= 0 \quad (x = 0, 1; \quad 0 \leqslant y \leqslant 1) \\ \psi_n &= 0 \quad (y = 0, 1; \quad 0 \leqslant x \leqslant 1) \end{aligned}\right\} \quad \text{for all } n, \tag{3.6}$$

$$\left.\begin{aligned} &\left.\begin{aligned} \psi_{n,y} &= 0 \quad (y = 0; \quad 0 \leqslant x \leqslant 1) \\ \psi_{n,x} &= 0 \quad (x = 0, 1; \quad 0 \leqslant y \leqslant 1) \end{aligned}\right\} \quad \text{for all } n, \\ &\psi_{n,y} = 0 \quad (y = 1; \quad 0 \leqslant x \leqslant 1; \quad n \neq \pm 1), \\ &\psi_{n,y} = \tfrac{1}{2} \quad (y = 1; \quad 0 \leqslant x \leqslant 1; \quad n = \pm 1). \end{aligned}\right\} \tag{3.7}$$

We now discretize the above system, using second-order finite differencing. If Δx and Δy are the mesh sizes in the x- and y-directions, then for example

$$\psi_{n,y}(x, y) = \frac{\psi_n(x, y + \Delta y) - \psi_n(x, y - \Delta y)}{2\Delta y} + O((\Delta y)^2), \tag{3.8a}$$

$$\psi_{n,xx}(x, y) = \frac{\psi_n(x + \Delta x, y) - 2\psi_n(x, y) + \psi_n(x - \Delta x, y)}{(\Delta x)^2} + O((\Delta x)^2). \tag{3.8b}$$

We next truncate the series (3.3) at $n = \pm N$, say, and so at any given x-station, for each n, the set of difference equations for $0 \leqslant y \leqslant 1$ may be expressed in the matrix form

$$\mathbf{L}_n \mathbf{x}_n = \mathbf{R}_n, \tag{3.9}$$

where $\mathbf{L}_n$ is a square matrix, each row of which contains just six elements centred around the diagonal (and is thus suitable for Gaussian elimination). To be rather more precise, $\mathbf{L}_n$ consists entirely of 2×6 submatrices, each submatrix corresponding to the differenced form of (3.5) (with each row of these submatrices corresponding to one of the equations (3.5)) at each y-station. As much of the left-hand side of (3.5) as possible was included in $\mathbf{L}_n$, the remaining quantities being included (along with all the right-hand-side terms) in the column vector $\mathbf{R}_n$. $\mathbf{x}_n$ is the column vector corresponding to the unknowns $\psi_n(x, y)$ and $\zeta_n(x, y)$ (x constant, $0 \leqslant y \leqslant 1$).

Because of (3.4), we need only consider $n = 0, 1, 2, \ldots, N$. Further, because of the

oscillatory nature of the forcing through the wall motion, and the symmetry of the motion about $x = \frac{1}{2}$, we must have

$$\psi(t+\pi, 1-x, y) = -\psi(t, x, y), \quad \zeta(t+\pi, 1-x, y) = -\zeta(t, x, y). \tag{3.10}$$

The outcome of this is that

$$\psi_{2n}(1-x, y) = -\psi_{2n}(x, y), \quad \zeta_{2n}(1-x, y) = -\zeta_{2n}(x, y), \tag{3.11a}$$

$$\psi_{2n-1}(1-x, y) = \psi_{2n-1}(x, y), \quad \zeta_{2n-1}(1-x, y) = \zeta_{2n-1}(x, y). \tag{3.11b}$$

From (3.11*a*) note that

$$\psi_{2n}(\tfrac{1}{2}, y) = \zeta_{2n}(\tfrac{1}{2}, y) = 0. \tag{3.12}$$

Equation (3.11) enables us to halve the domain of x we need to consider; hence we solve in just $0 \leqslant x \leqslant \frac{1}{2}$.

The treatment of ζ near the walls also requires a certain amount of attention, although here we may follow Burggraf (1966). The problem arises because ζ_n is not prescribed on the walls, whilst the difference equations that are set up at $y = \Delta y$ and $y = 1-\Delta y$ require $\zeta_n(x, 0)$ and $\zeta_n(x, 1)$ respectively. Considering first the lower wall, from our definition of ζ_n

$$\zeta_n(x, 0) = -\frac{\psi_n(x, \Delta y) - 2\psi_n(x, 0) + \psi_n(x, -\Delta y)}{(\Delta y)^2}. \tag{3.13}$$

But $\psi_n(x, 0) = 0$, and also

$$\psi_n(x, -\Delta y) = \psi_n(x, \Delta y)$$

(since $\psi_{n,y}(x, 0) = 0$), and so

$$\zeta_n(x, 0) = -2\psi_n(x, \Delta y)/(\Delta y)^2. \tag{3.14}$$

(An alternative to (3.14), which may also be used, comes directly from the no-slip condition on the wall, namely $\psi_n(x, \Delta y) = \frac{1}{4}\psi_n(x, 2\Delta y)$.)

The treatment on the upper wall for $n \neq \pm 1$ is identical, but for $n = \pm 1$ is slightly changed since $\psi_{\pm 1, y}(x, 0) = \frac{1}{2}$. As a result

$$\zeta_{\pm 1}(x, 1) = -2\psi_{\pm 1}(x, 1-\Delta y)/(\Delta y)^2 - 1/\Delta y. \tag{3.15}$$

(Alternatively we may use $\psi_{\pm 1}(x, 1-\Delta y) = \frac{1}{4}\psi_{\pm 1}(x, 1-2\Delta y) + \frac{1}{4}\Delta y$.)

Notice that $\zeta_n(0, y)$, which is required at the $x = \Delta x$ station, may be obtained in exactly the same manner as (3.14) to give

$$\zeta_n(0, y) = -2\psi_n(\Delta x, y)/(\Delta x)^2. \tag{3.16}$$

The iteration procedure adopted was to start at $x = \Delta x$, to solve for the entire range of y (i.e. (3.9)) for each successive n, then to move to $x = 2\Delta x$, and to repeat the process until $x = \frac{1}{2}$ is reached. At all times the latest information available was used in the difference scheme (i.e. the iterative scheme was of a line Gauss–Seidel form, although as described later the more difficult examples required a certain amount of under-relaxation). At $x = \frac{1}{2}$ it is only necessary to solve for the odd-n terms, as a result of (3.12), and we use the symmetry condition in the following manner:

$$\psi_{2n-1}(\tfrac{1}{2} + \Delta x, y) = \psi_{2n-1}(\tfrac{1}{2} - \Delta x, y), \quad \zeta_{2n-1}(\tfrac{1}{2} + \Delta x, y) = \zeta_{2n-1}(\tfrac{1}{2} - \Delta x, y). \tag{3.17}$$

Having obtained a solution at $x = \frac{1}{2}$, we then repeat the process until convergence is obtained.

As a final general check of the computer program, a number of the steady examples of Burggraf (1966) were used (the program needed only minor modifications for this purpose, although the aforementioned symmetries do not exist) and was found to produce satisfactory agreement.

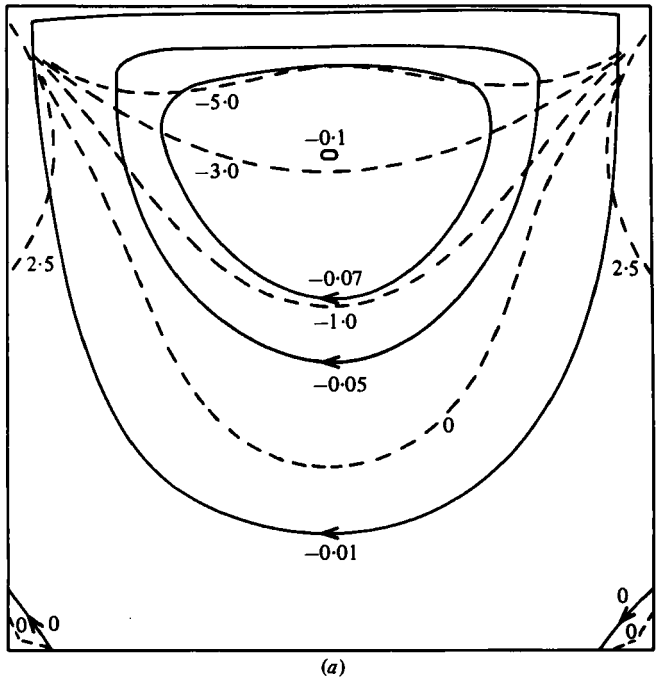

(a)

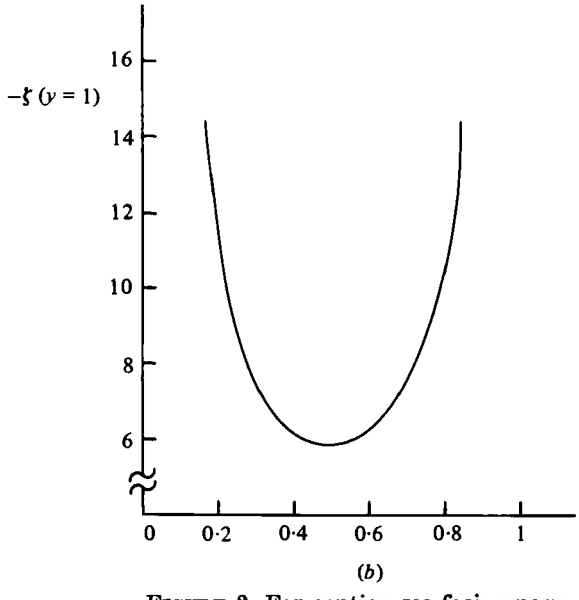

(b)

FIGURE 2. For caption see facing page.

4. Results and discussion

The first set of results (figures 2*a–d*) correspond to the example $R = 0, \beta = 1$, and so represent physically a very small-amplitude, fairly low-frequency oscillation of the upper wall. Because of the lack of inertia terms (since $R = 0$), the system (3.1), (3.2) is linear, with $n = \pm 1$ being the only non-zero terms in (3.3), and so (3.5) reduces to

$$\pm i\beta\zeta_{\pm 1} = \nabla^2\zeta_{\pm 1}. \tag{4.1}$$

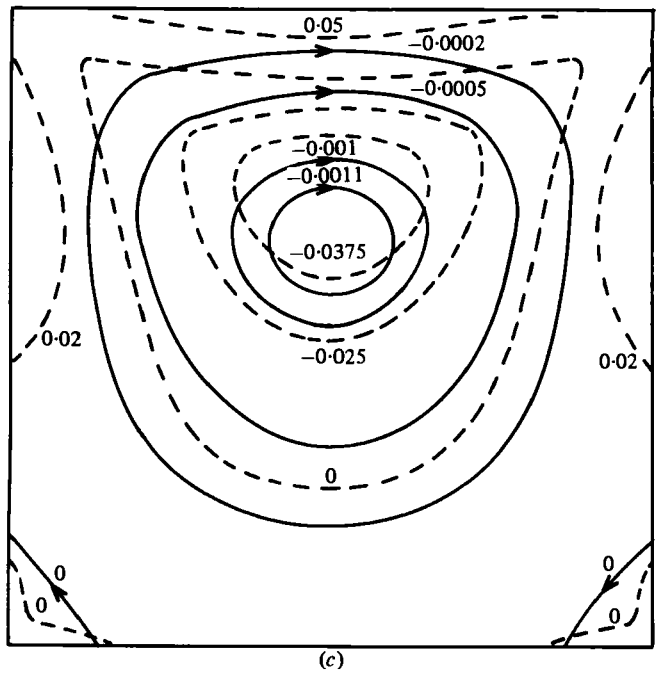

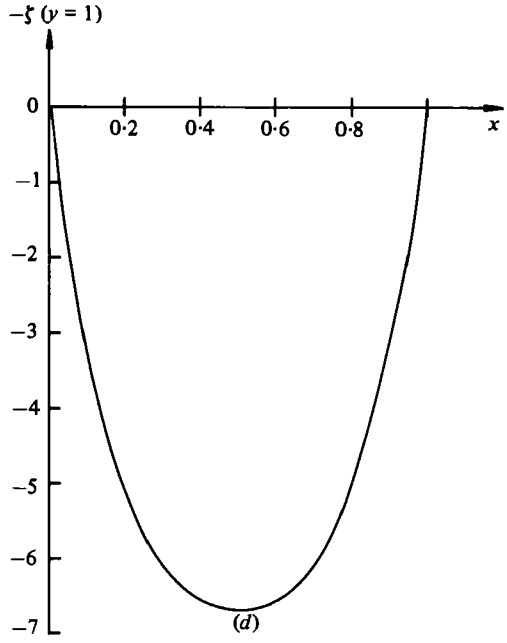

FIGURE 2. (*a*) Streamlines (solid lines) and constant-vorticity lines (broken lines) at $t = 0$ ($\beta = 1$, $R = 0$). (*b*) Upper wall shear at $t = 0$ ($\beta = 1$, $R = 0$). (*c*) Streamlines (solid lines) and constant-vorticity lines (broken lines) at $t = \frac{1}{2}\pi$ ($\beta = 1$, $R = 0$). (*d*) Upper wall shear at $t = \frac{1}{2}\pi$ ($\beta = 1$, $R = 0$).

In spite of the linear nature of this system, analytic solutions in closed form appear not to be possible by standard methods. Indeed, this also applies to the corresponding steady example, although Burggraf (1966) did attempt to use an approximate conformal-mapping technique, following Muskhelishvili (1963), but found that in general finite-difference methods were preferable.

Because the solution of (4.1) involves the study of just one Fourier term, it was feasible to use a particularly small finite-difference grid size in this example, in both the x- and y-directions, namely $\Delta x = \Delta y = 0{\cdot}0125$. Figure 2($a$) (solid lines) shows the plot of selected streamlines at the time $t = 0$, corresponding to the instant when the moving wall possesses its greatest velocity, namely of value unity directed along the positive x-direction. In addition to one main eddying motion, we see a small region of contrarotating fluid, in both the lower corners of the cavity. Such a phenomenon is commonly observed in the steady case. Figure 2(a) also shows the corresponding selected lines of constant vorticity (broken lines), and figure 2(b) is a plot of the distribution of vorticity (and hence wall shear) on the upper (moving) wall at $t = 0$. Note that for $R = 0$ all stream-function and vorticity distributions will be symmetrical about $x = \frac{1}{2}$, and also

$$\psi(t+\pi, x, y) = -\psi(t, x, y), \quad \zeta(t+\pi, x, y) = -\zeta(t, x, y). \tag{4.2}$$

Figures 2(c, d) correspond to figures 2(a, b) respectively, but are evaluated at the time $t = \frac{1}{2}\pi$, the instant when the upper wall is at rest (and about to move in the negative x-direction), and so the motion is a measure of the time lag in the fluid motion. At this particular instant, the motion appears to be considerably weaker than at $t = 0$. This may be explained by considering the limit $\beta \to 0$, which is the quasisteady limit. For $\beta = 0$, the results of Burggraf (1966) apply instantaneously, and consequently if the upper wall were at rest there would be no fluid motion. The results for $t = 0$ correspond, remarkably, with the results of Burggraf (1966) for $R = 0$, and so the solution for $\beta = 1$ appears quasisteady to a good approximation.

The neighbourhoods of the two upper corners appear to be regions of high solution gradient (see for example figure 2b). It is to be expected that the flow in these regions is described by the (steady) corner-flow solutions of Dean & Montagnon (1949) and Moffatt (1964) (note that such analysis is valid for unsteady flows sufficiently close to the corner). Accordingly, if we assume that the flow in the region of the corner is governed by Stokes' equation (i.e. acceleration terms are negligible), which is a rational assumption if the solution is analytic in this region, then, following Moffatt (1964), the stream function near the corner $x = 0$, $y = 1$ (for example) may be written as

$$\psi = \frac{r \cos t}{1 - \frac{1}{4}\pi^2}[\theta \cos\theta - \tfrac{1}{2}\pi(\theta + \tfrac{1}{2}\pi)\sin\theta] + O(\beta r^3), \tag{4.3}$$

where

$$\theta = \arctan\frac{y-1}{x}, \quad r = [x^2 + (y-1)^2]^{\frac{1}{2}}. \tag{4.4}$$

The error involved in neglecting the acceleration terms is $O(\beta r^3)$, and so, as the oscillation increases in frequency, the region of validity for which Stokes' equation is valid decreases. It is likely, also, that the further results given by Moffatt (1964) pertaining to flows near corners apply near both the lower cavity corners. Similar eddies were found in the corresponding steady-flow problem by Burggraf (1966) and also by Pan & Acrivos (1967). The latter authors did an extensive investigation into

these eddies for zero Reynolds numbers, and found a sequence of smaller and smaller corner vortices (in excellent agreement with the theory of Moffatt (1964)). It would appear probable that a similar sequence occurs in the present problem, but that the resolution of the finite-difference scheme is insufficient to reveal their existence.

The next set of results (figures 3*a–d*) corresponds to $R = 0$, $\beta = 100$, and so again it was just necessary to consider one Fourier term (again a mesh size of 0·0125 was used in both the x- and y-directions), and the remarks concerning the various symmetries of the previous set of results again apply. Comparing the flow at $t = 0$, as shown in figures 3(a, b), with the corresponding figures of the previous set of results, we see that the general trend is an overall weakening of the flow away from the moving wall. For example the main eddying motion is weaker in magnitude, whilst its centre has moved towards the upper wall. A further difference is that the contrarotating regions of fluid, whilst still present at the two lower corners of the cavity, are reduced significantly in size. The general trend as $\beta \to \infty$ appears to be a concentration of the flow within a boundary layer on the upper wall, with a reduction in the flow throughout the cavity away from this wall.

An inspection of the various quantities in the Navier–Stokes equations of motion as $\beta \to \infty$ suggests (away from the two vertical walls $x = 0$, $x = 1$) a balance between the horizontal acceleration term, and the (dominant) viscous term to give

$$\beta\psi_{yyt} \sim \psi_{yyyy}.$$

Defining a new vertical lengthscale

$$Y = \beta^{\frac{1}{4}}(1-y) = O(1), \tag{4.5}$$

then

$$\psi_{YYt} - \psi_{YYYY} = 0, \tag{4.6}$$

which is Stokes' (unsteady) equation. If we now assume that in the limit $\beta \to \infty$ the motion in the core of the cavity disappears (to leading order), a result suggested by our numerical results, then we may impose the boundary condition

$$\psi_Y \to 0 \quad \text{as} \quad Y \to \infty. \tag{4.7}$$

Equation (4.7), in conjunction with the conditions on $Y = 0$, namely

$$\psi = 0, \quad \psi_Y = -\beta^{-\frac{1}{4}} \cos t, \tag{4.8}$$

yields the following solution for the streamfunction:

$$\psi = \frac{1-i}{2(2\beta)^{\frac{1}{4}}}[e^{-(1+i)Y/\sqrt{2}} - 1]e^{it} + \text{complex conjugate}, \tag{4.9}$$

which is a form of Stokes' (unsteady) solution. Although the flow in the vicinity of the corner regions will be more complicated (partly described by (4.3)), (4.9) does provide an insight into the high-frequency limit, suggested by the results of figure 3.

The thinning of the boundary layer is predicted because of the scaling (4.5), which indicates that the boundary layer reduces as $\beta^{-\frac{1}{4}}$. In addition this gives a measure of the reliability of our numerical results. We may expect a boundary-layer thickness $O(0{\cdot}1)$, whilst our mesh size is 0·0125, and so there should be a reasonable resolution of the boundary-layer profile by our finite-difference scheme. Equation (4.9) also suggests little horizontal variation in the flow near $y = 1$ (away from the two vertical walls), a feature clearly observed in figure 3(a).

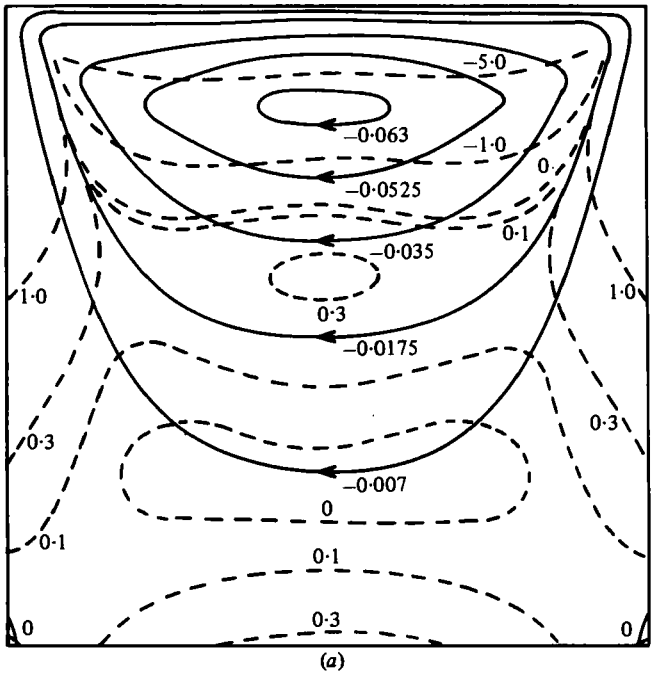

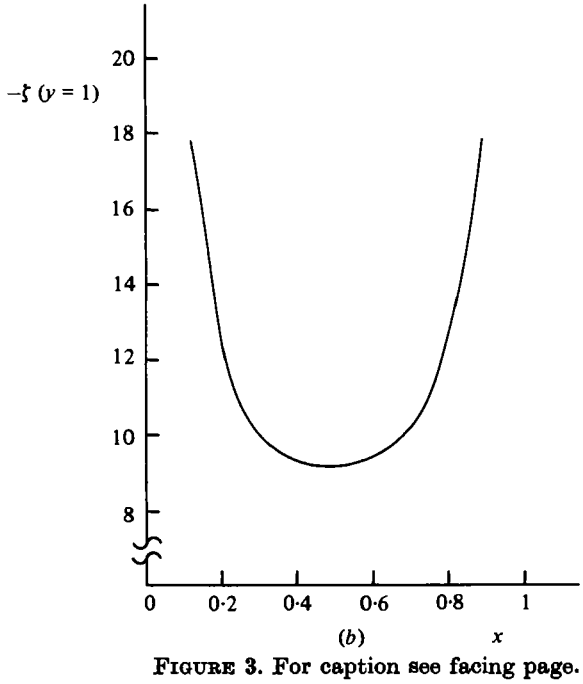

FIGURE 3. For caption see facing page.

The flow for $R = 0$, $\beta = 100$ at $t = \frac{1}{2}\pi$ is illustrated in figures 3(*c*, *d*), and appears rather weaker than the flow at the previous time $t = 0$. However, in contrast to the solution for $t = 0$, the flow at $t = \frac{1}{2}\pi$ is quite markedly stronger than that for $\beta = 1$ at $t = \frac{1}{2}\pi$. The physical explanation of this would appear to be that, at the higher frequency parameter of $\beta = 100$, the greater importance of the acceleration terms in the equations

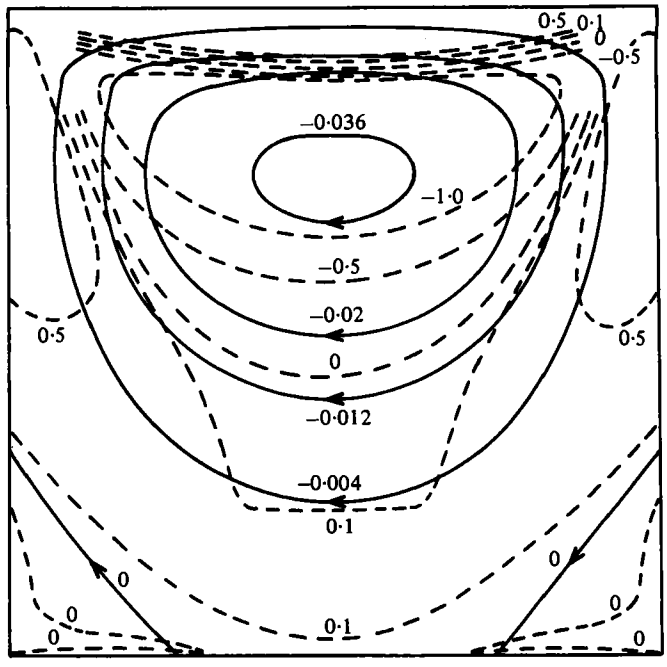

(*c*)

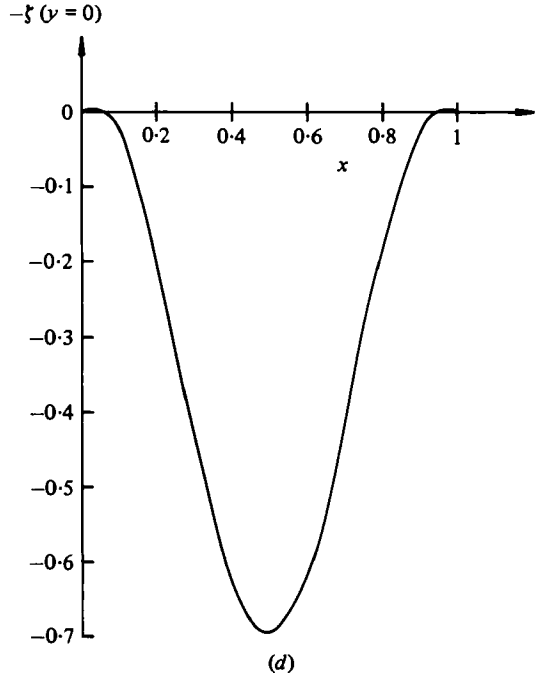

(*d*)

FIGURE 3. (*a*) Streamlines (solid lines) and constant-vorticity lines (broken lines) at $t = 0$ ($\beta = 1$, $R = 0$). (*b*) Upper wall shear at $t = 0$ ($\beta = 100$, $R = 0$). (*c*) Streamlines (solid lines) and constant-vorticity lines (broken lines) at $t = \frac{1}{2}\mu$ ($\beta = 100$, $R = 0$). (*d*) Upper wall shear at $t = \frac{1}{2}\pi$ ($\beta = 100$, $R = 0$).

of motion introduces more 'lag' in the flow, compared with the comparatively quasisteady results of $\beta = 1$, and this effect offsets the other trend of weakening of the flow away from the moving walls.

We now go on to consider a number of sets of results for non-zero Reynolds numbers. Before actually considering these solutions in detail, it is useful to note a number of details, in particular differences from the $R = 0$ results.

Because all Fourier terms are triggered through the nonlinearity of the governing equations, computing times were significantly longer, and for this reason a rather coarser grid size was used in the finite-difference scheme ($\Delta x = \Delta y = 0{\cdot}025$). In order to keep a check on the accuracy, in every case, a control computation was used, using an even coarser grid ($\Delta x = \Delta y = 0{\cdot}05$). In all cases five Fourier terms were computed (equivalent to using nine terms in (3.3) because of the property (3.4)), adding an extra term to the highest Reynolds number tackled resulted in a change of no more than 2 % in the most sensitive regions, namely the upper corner regions, and considerably less in the rest of the flow field. Approximately 800 iterations were required for five-figure accuracy of convergence. Particularly at high Reynolds numbers, the iterative scheme appeared to become less stable and, as an aid to convergence, a certain amount of under-relaxation was applied, where, instead of updating the stream function completely by the latest computed value ψ_n^{comp}, the following formula was used:

$$\psi_n(x,y) = f\psi_n^{\text{old}}(x,y) + (1-f)\,\psi_n^{\text{comp}}(x,y), \tag{4.10}$$

where ψ_n^{old} was the previous value and f is the relaxation parameter (a similar formula was used for $\zeta_n(x,y)$). Typically $f = 0{\cdot}6$ was chosen (although no exhaustive optimization process was carried out).

Results will be presented, as before, at $t = 0$ and $t = \frac{1}{2}\pi$; however, the property (3.10) enables us to use these two sets of results to obtain distributions every $\frac{1}{2}\pi$ interval throughout the entire period of the oscillation. Note that the inclusion of inertia terms destroys the rather simple antisymmetry condition (4.2) and also the general symmetry about $x = \frac{1}{2}$ present when $R = 0$.

One final point of detail is that, in all the preceding sets of computation, we have deliberately chosen $\beta = R$. With this condition, it is to be expected that there will be the maximum amount of interaction between the various physical processes. If $\beta \ll R$, then we may expect that the flow will become quasisteady (with the results of Burggraf (1966) applying instantaneously), whilst, for $\beta \gg R$, our previous results for $R = 0$ suggest that the flow will become concentrated within a boundary layer on the moving wall.

Figures 4 (*a–d*) relate to the point in parameter space $R = \beta = 200$. Compared to the previous results, there appears a further general weakening of the flow in the main body of the fluid, along with a further intensification of the flow inside the boundary layer situated on the upper wall. This boundary layer is likely to be of thickness $O(R^{-\frac{1}{2}}) \sim O(\beta^{-\frac{1}{2}}) \sim O(0{\cdot}07)$. At $t = 0$ (figure 4*a*) the centre of the main eddying motion appears to have moved to the right of centre of the cavity, and further towards the upper wall. The two small regions of contrarotating flow in the two lower corners observed previously seem to have disappeared (or are too small to be resolved by the finite-difference scheme), whilst at $t = \frac{1}{2}\pi$ (figure 4*b*) these two regions have reappeared, the left-hand example of which extends along the entire length of the left-hand vertical wall.

Particularly interesting in problems of this type is the steady streaming motion. Although the fluid is forced in a purely oscillatory manner, the nonlinearity of the inertia terms in the Navier–Stokes equations provides a mechanism for forcing a steady component of motion. Because of the antisymmetry condition (3.11*a*), the streamlines and constant-vorticity lines corresponding to this steady streaming are only shown in the left-hand side of the cavity. This component of motion (figure 4*c*) is seen to take on the form of two main contrarotating eddies, with two further medium-sized, but weaker eddies, one in the region of each lower corner. Also shown (figure 4*d*) is the distribution of the steady component of wall shear on the moving wall, which for most of the length of the wall takes on a linear distribution.

Figures 5(*a–d*) correspond to the parameters $R = \beta = 400$. At $t = 0$ (figure 5*a*) a further eddy has appeared on the left-hand wall of the cavity, whilst the primary eddy has reduced (further) in strength. At $t = \frac{1}{2}\pi$ (figure 5*b*), the flow is little changed from the $R = \beta = 200$ results, except for the continued trend of a weakening of the flow away from the upper wall (and a strengthening of the flow near the upper wall). Figure 5(*c*) reveals that the main steady streaming eddy is little changed from before, whilst the lower eddy has increased in size. The distribution of steady wall shear (figure 5*d*) takes on a similar linear distribution to that observed previously (figure 4*d*), but possesses a larger gradient than before.

Figures 6(*a–d*) relate to the final example tackled, $R = \beta = 600$. Figures 6(*a*, *b*) present a similar pattern to figures 5(*a*, *b*), whilst continuing the previous trend of a weakening of the flow throughout most of the cavity, but with an increase in intensity of the flow near the upper wall. Figure 6(*c*) shows that the steady streamlines and constant-vorticity lines also exhibit this trend when compared with figure 5(*c*) whilst, in figure 6(*d*), the steady component of wall shear takes on the linear distribution with x observed in the two previous cases, but again possesses an increased gradient.

Inspection of figures 4(*d*), 5(*d*) and 6(*d*) suggests that the steady wall shear varies approximately as $R^{\frac{1}{2}}$. This may be explained mathematically, since in the neighbourhood of the upper wall the horizontal velocity is (generally) $O(1)$, whilst the typical vertical lengthscale, using similar arguments to those used in deriving (4.5), is likely to be $O(\beta^{-\frac{1}{2}}) \sim O(R^{-\frac{1}{2}})$, and the variation of wall shear as $R^{\frac{1}{2}}$ then follows.

No further computations were carried out past $R = \beta = 600$, since with this choice of parameter the (maximum) discrepancy between the actual computation and the control computation was approximately 10 %, and it was felt that any further calculations at higher Reynolds numbers would be of dubious accuracy. The breakdown of solution beyond $R = \beta = 600$ may be explained by the boundary-layer thickness ($O(R^{-\frac{1}{2}}) \sim O(0{\cdot}04)$), which is comparable to the control grid size ($O(0{\cdot}05)$). However, as noted previously, an additional term in the Fourier-series representation of the stream function and vorticity made little difference to the solution, and the method appears to be an efficient approach to the problem. Such an approach could also be used for situations involving more general periodic motions of the upper wall (such as pulsatile movements), although certain of the useful symmetries present in the oscillatory case considered here (which halve the range of x that need be considered) would be lost.

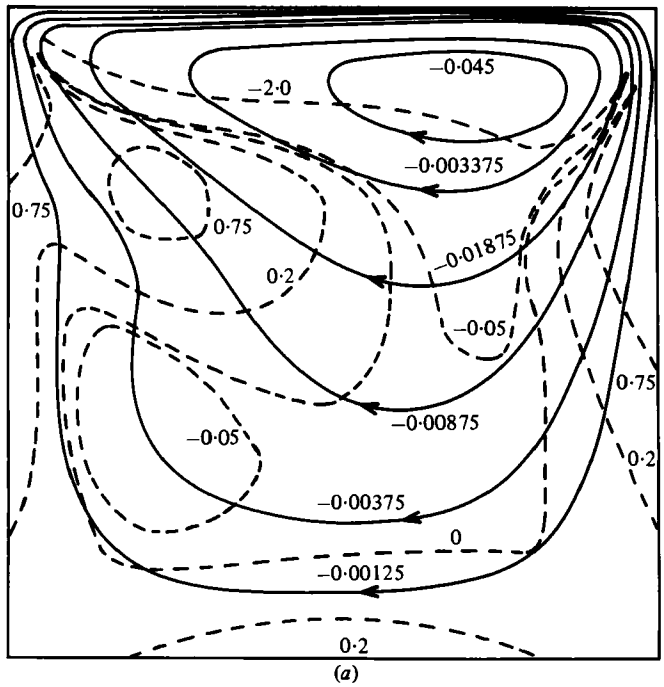

(a)

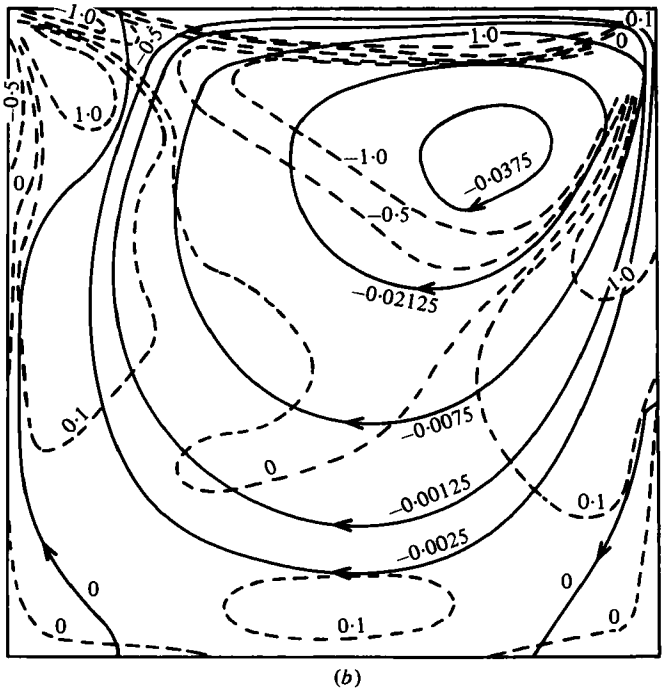

(b)

FIGURE 4. For caption see facing page.

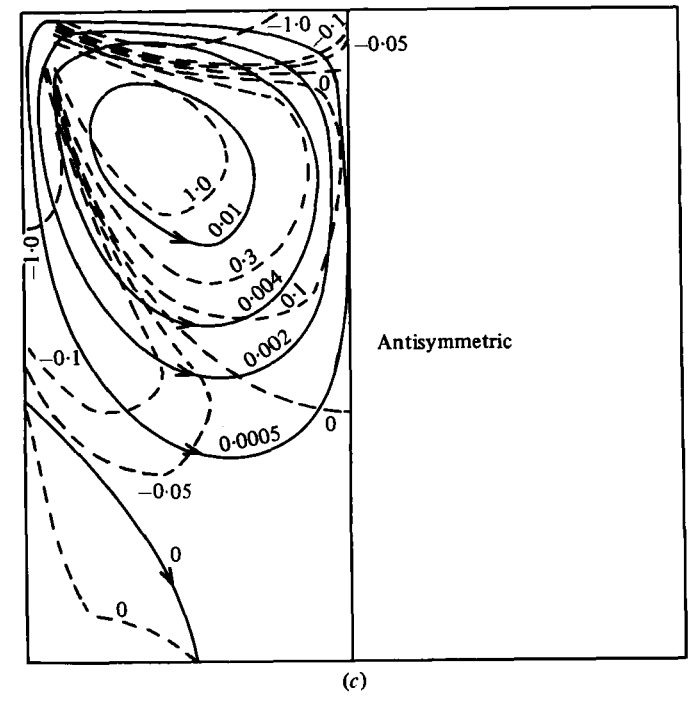

(*c*)

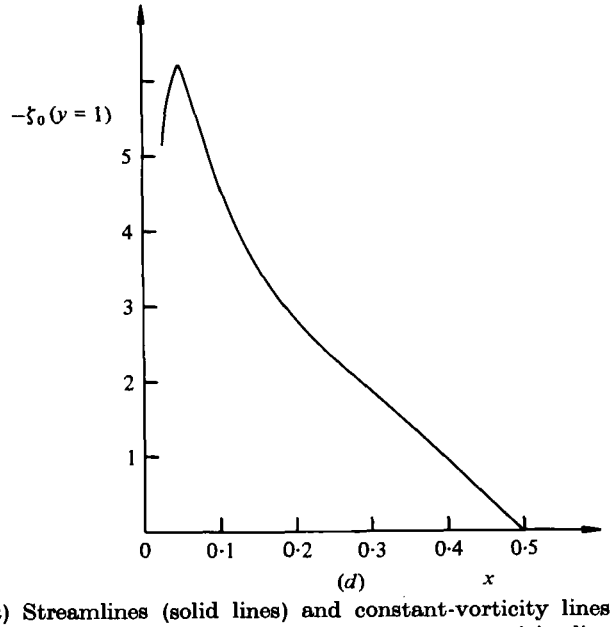

(*d*)

FIGURE 4. (*a*) Streamlines (solid lines) and constant-vorticity lines (broken lines) at $t = 0$ ($\beta = R = 200$). (*b*) Streamlines (solid lines) and constant-vorticity lines (broken lines) at $t = \frac{1}{2}\pi$ ($\beta = R = 200$). (*c*) Steady streaming streamlines (solid lines) and constant-vorticity lines (broken lines) ($\beta = R = 200$). (*d*) Steady streaming upper wall shear ($\beta = R = 200$).

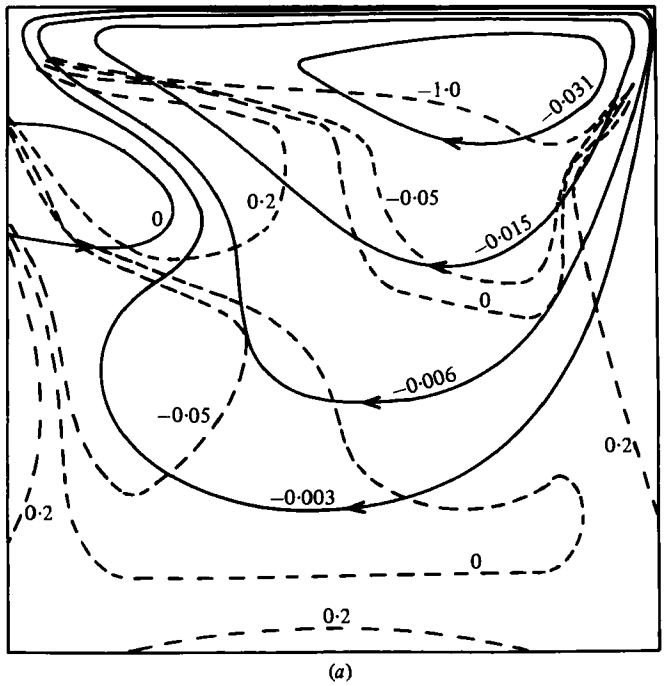

(a)

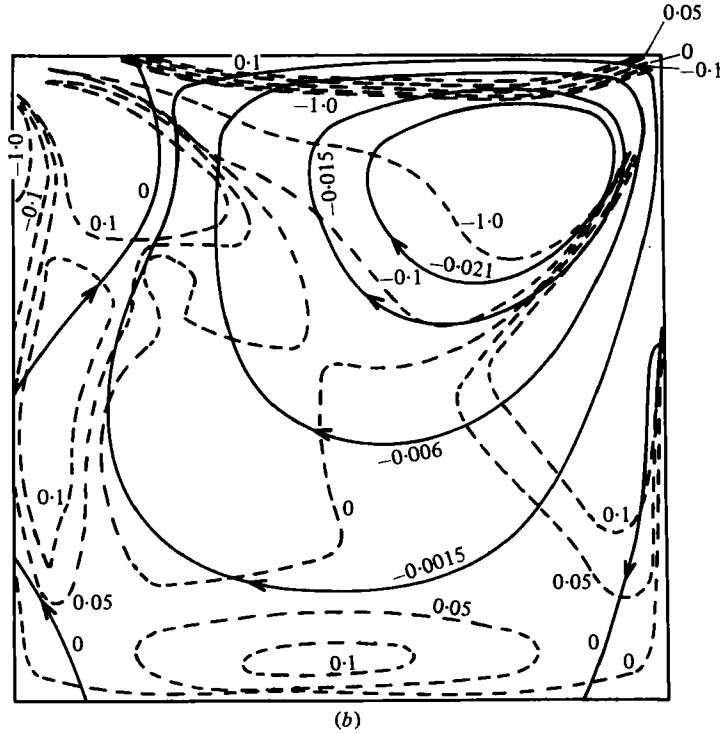

(b)

FIGURE 5. For caption see facing page.

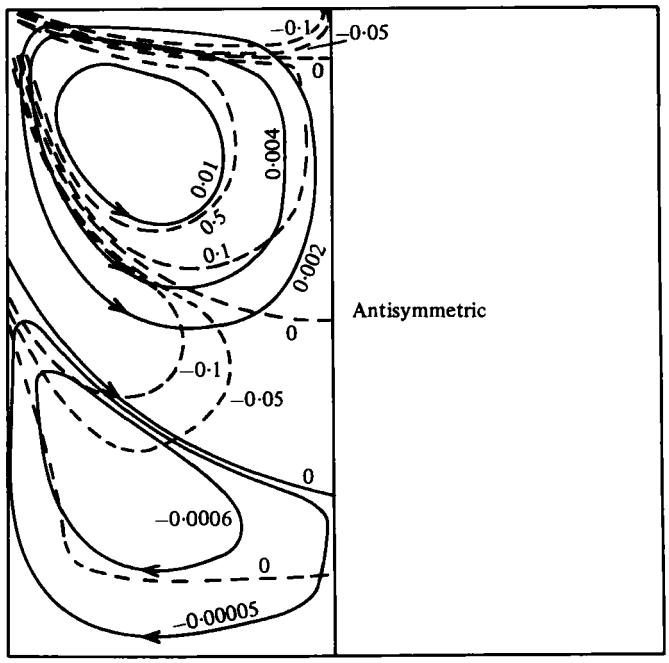

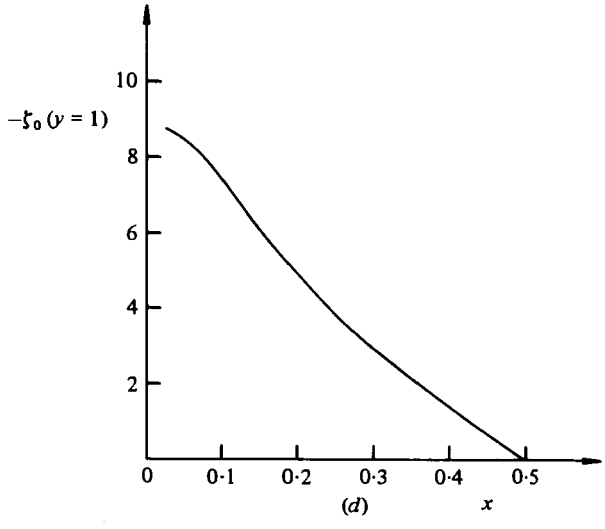

FIGURE 5. (*a*) Streamlines (solid lines) and constant-vorticity lines (broken lines) at $t = 0$ ($\beta = R = 400$). (*b*) Streamlines (solid lines) and constant-vorticity lines (broken lines) at $t = \frac{1}{2}\pi$ ($\beta = R = 400$). (*c*) Steady streaming streamlines (solid lines) and constant-vorticity lines (broken lines) ($\beta = R = 400$). (*d*) Steady streaming upper wall shear ($\beta = R = 400$).

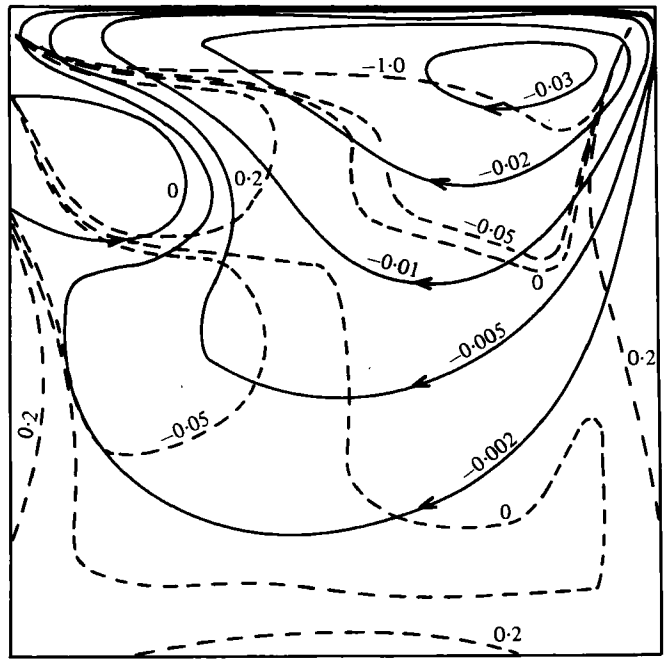

(*a*)

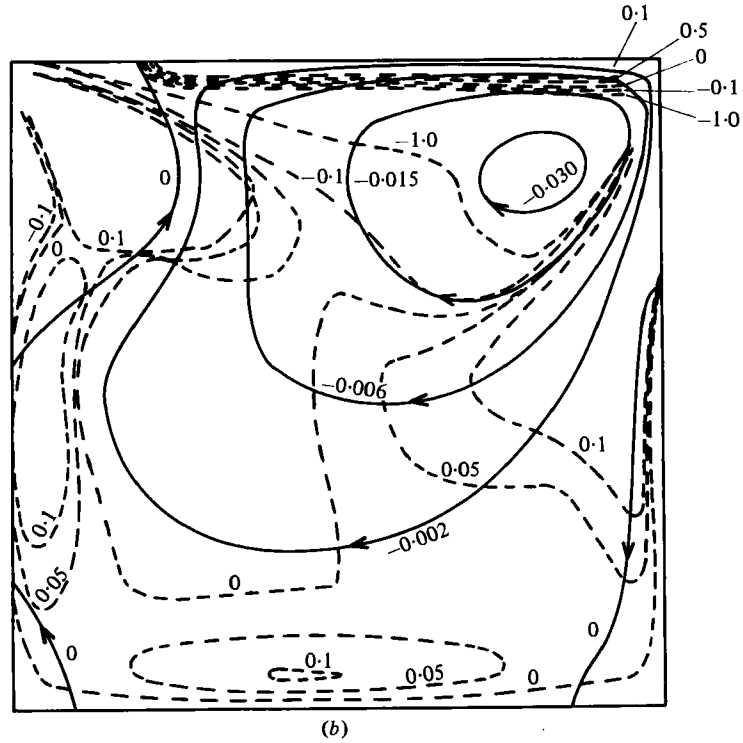

(*b*)

FIGURE 6. For caption see facing page.

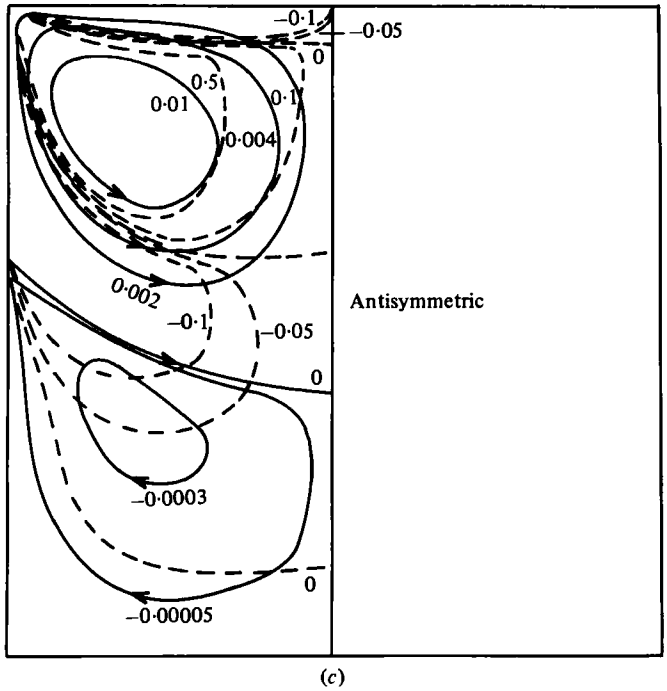

(*c*)

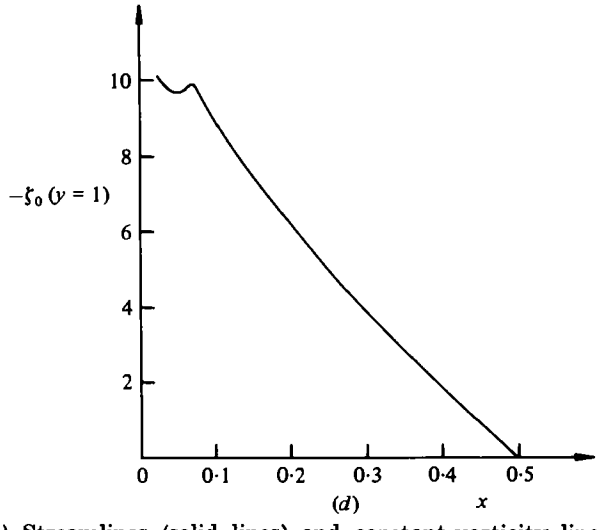

(*d*)

FIGURE 6. (*a*) Streamlines (solid lines) and constant-vorticity lines (broken lines) at $t = 0$ ($\beta = R = 600$). (*b*) Streamlines (solid lines) and constant-vorticity lines (broken lines) at $t = \frac{1}{2}\pi$ ($\beta = R = 600$). (*c*) Steady streaming streamlines (solid lines) and constant-vorticity lines (broken lines) ($\beta = R = 600$). (*d*) Steady streaming upper wall shear ($\beta = R = 600$).

REFERENCES

BATCHELOR, G. K. 1956 *J. Fluid Mech.* **1**, 177.

BERTELSEN, A. F. 1974 *J. Fluid Mech.* **64**, 389.

BURGGRAF, O. R. 1966 *J. Fluid Mech.* **24**, 113.

DEAN, W. R. & MONTAGNON, P. E. 1949 *Proc. Camb. Phil. Soc.* **45**, 309.

DUCK, P. W. & SMITH, F. T. 1979 *J. Fluid Mech.* **91**, 93.

GREENSPAN, D. 1968 *Lectures on the Numerical Solution of Linear, Singular and Nonlinear Differential Equations*. Prentice-Hall.

KAWAGUTI, M. 1961 *J. Phys. Soc. Japan* **16**, 2307.

LYNE, W. H. 1971 *J. Fluid Mech.* **50**, 33.

MOFFATT, H. K. 1964 *J. Fluid Mech.* **18**, 1.

MUSKHELISHVILI, N. I. 1963 *Some Basic Problems of the Mathematical Theory of Elasticity*. Noordhoff.

PAN, F. & ACRIVOS, A. 1967 *J. Fluid Mech.* **28**, 643.

RILEY, N. 1965 *Mathematika* **12**, 161.

RILEY, N. 1967 *J. Inst. Math. Applics* **3**, 419.

SHAY, W. A. 1981 *Computers and Fluids* **9**, 279.

SIMUNI, L. M. 1964 *Inzhenernii Zh* (*USSR*) **4**, 446.

STUART, J. T. 1966 *J. Fluid Mech.* **24**, 673.

TUANN, S. Y. & OLSON, M. D. 1978 *J. Comp. Phys.* **29**, 1.

VAHL DAVIES, G. DE & MALLINSON, G. D. 1976 *Computers and Fluids* **4**, 29.